Journal of Visualization, Vol. 1, No. 3 (1999) 303-312

3-D Airflow Measurement Using Smoke Particles

Kaga, A.*, Yamaguchi, K.*, Inoue, Y.* and Kondo, A.*

*Department of Environmental Engineering, Osaka University, 2-1 Yamadaoka, Suita-shi, Osaka, 565-0871 Japan.

Received 12 March 1998.
Revised 18 August 1998.

***Abstract*:** A new 3-D PIV-technique that is applicable to low velocity airflow in a real space such as indoor airflow is proposed, and its performance is inspected through a simulation and an experimental application. In this technique, two parallel planes separated by short distance are illuminated by a pair of laser light sheets of different colors. The visualized images are separated with optical filters, and recorded on VTRs. The 2-D tracer pattern movement on visualized planes is tracked with pattern tracking and the movement normal to the visualized planes is calculated from the difference of tracer concentration between two planes. The simulation result showed that the algorithm proposed here can calculate 3-D velocity field adequately, but the experimental result showed that the luminous intensity difference between two visualized planes became the main source of experimental errors.

***Keywords*:** PIV, indoor airflow, pattern tracking, simulation, wind tunnel experiment.

***Nomenclature*:**

D	summation of gray level difference between corresponding pixels
f, g	gray level of a pixel
n_M	image fragment size
S	light sheet distance
t	time
u, w	velocity components on visualized planes
v	velocity component normal to visualized planes
x, y, z	coordinate in space
Δt	sampling time step
Δx	x-displacement of fluid during Δt
Δy	y-displacement of fluid during Δt
ξ, η	coordinate on image

1. Introduction

We have reported that video-base pattern tracking using smoke or mist particles as tracer particles is useful to measure low velocity airflow in a real space (Kaga, et al., 1993), but the application has been limited to be 2-D. In this paper, we propose a new technique to measure 3-D velocity field by calculating velocity component normal to the visualized plane from gray level difference between two visualized planes normal to the camera axis.

In particle tracking, tracer particles at different depth are visualized simultaneously, and their movement can be tracked independently. In pattern tracking, on the contrary, fine tracer particles exist densely on a visualized plane and they move in a body. Therefore, it is difficult to obtain the information at different depth in pattern tracking, and the reports treating 3-D measurement using pattern tracking are few.

Kimura and Kohono (1991) observed two different cross sections illuminated by different color light as

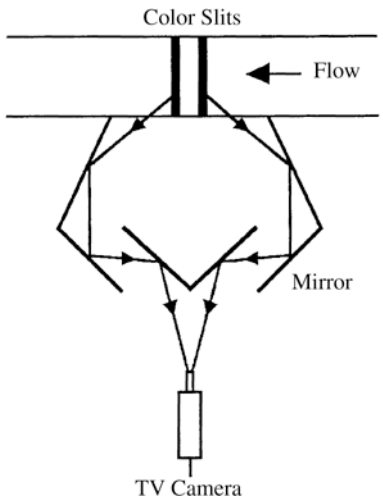

Fig. 1. Spatio-temporal correlation method (Kimura and Kohono, 1991).

shown in Fig. 1. The color camera image was separated to two cross sectional images using color information, and the spatio-temporal correlation factors were calculated between two images to obtain 3-D velocity vectors. In this technique, the visualized planes were normal to the main flow direction, and therefore the tracer particles were supplied to the whole space.

But the life of tracers for airflow such as mist or smoke particles is much shorter compared with tracers for water flow, and it is difficult to fill the whole space with tracer particles. Tracer particles are usually supplied locally by predicting flow direction and the plane that is expected to include main flow is illuminated by a light sheet. The arrangement of visualized plane and a tracer generator shown in Fig. 2 is usual.

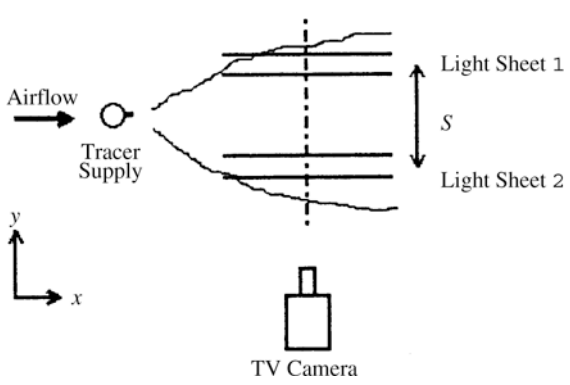

Fig. 2. Practical arrangement of visualized plane.

In this paper, we propose an algorithm to calculate 3-D velocity component from visualized images obtained in the arrangement of Fig. 2. Because the information at different depth is required to measure 3-D velocity field, two parallel planes separated by short distance S are illuminated with two laser light sheets of different colors and their images are recorded simultaneously.

2. Calculation of 2-D Components on Visualized Planes

Our tracking algorithm that have been used in 2-D measurement uses the summation of gray level difference given by

$$D=\sum_{i=1}^{n_M^2}\left|f_i-g_i\right| \tag{1}$$

as the similarity index of two image fragments (Fig. 3), and saves computation time by abandoning successively unpromising candidates on the way of calculation through a statistical inspection (Successive Abandonment)(Kaga, et al., 1993. Although the same tracking algorithm is used in this study to calculate 2-D velocity components on visualized planes, the procedure is modified as follows.

Although the image fragment corresponding to the fragment on image ① in Fig. 4 is looked for only on image ③ in the tracking to measure 2-D flow, it is not sufficient for a flow that has velocity component normal to the visualized plane. Therefore the images on 2-planes at 3-times are used here to find the most similar fragment couple among image pairs ① – ③, ① – ④, ① – ⑥, ② – ③ and ② – ⑤ to get a solution.

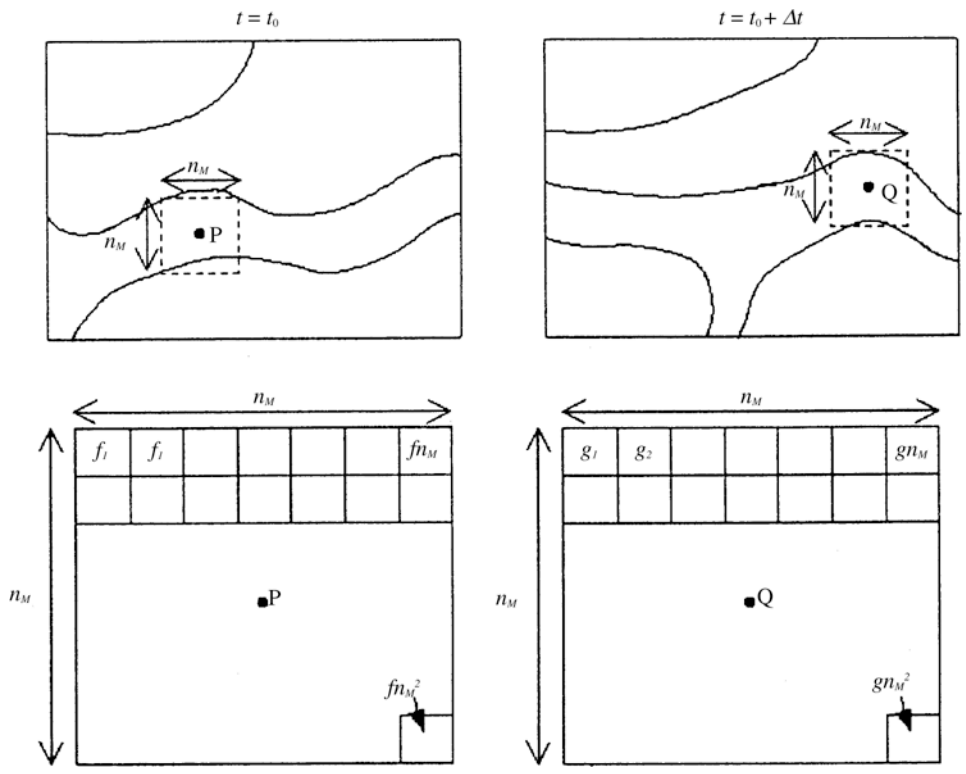

Fig. 3. Pair of image fragment to be identified in pattern tacking.

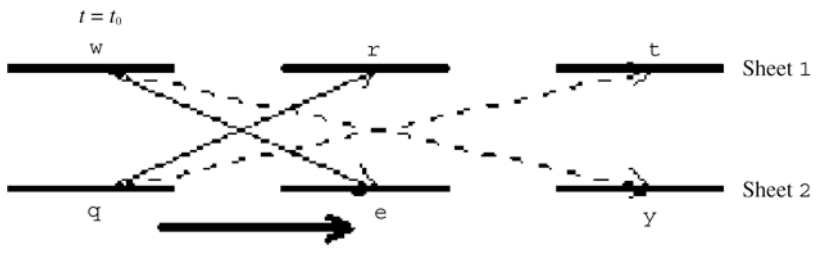

Fig. 4. Images used in tracking on visualized planes.

3. Calculation of Component Normal to Visualized Planes

Since the arrangement of Fig. 2 assumes the coincidence of visualized plane and main flow direction, the velocity component normal to visualized planes can be assumed to be small. The algorithm described here assumes the relationship,

$$\Delta y = v\Delta t \leq S \tag{2}$$

Suppose point P_1 at time $t = t_0$ in Fig. 5 moves to point P_1^* at time $t = t_0 + \Delta t$, without changing its tracer concentration. The points P_3 and P_4 that are the projected points of point P_1^* on visualized planes have already been obtained through pattern tracking on visualized planes. Therefore, if the distance S is short enough and the tracer concentration change between P_3 and P_4 can be assumed to be linear, then the point P_1^* is obtained as the position whose concentration coincides to the concentration of point P_1 on line L. Therefore the displacement Δy is given by

$$\Delta y = \frac{f_{P1} - f_{P3}}{f_{P4} - f_{P3}} \tag{3}$$

Here f_{Pi} represents the gray level of point P_i. Equation (3) holds even if the assumption of inequality Eq.(2) is not satisfied, but in this case, the position of point P_1^* is calculated by not interpolation but extrapolation and the error included will be increased. Although the relationship of Eq. (3) holds in each three pixels, image fragments similar to 2-D measurement are considered around P_1, P_3 and P_4, in practice, and the regression equation,

$$\Psi = \frac{\Delta y}{S} \Phi \tag{4}$$

is fitted to all the pixels on these fragments to reduce the influence of data scattering(Fig. 6). Here,

$$\begin{aligned} \Phi &= f_{P4} - f_{P3} \\ \Psi &= f_{P1} - f_{P3} \end{aligned} \tag{5}$$

and f_{Pi} represents gray levels of pixels in an image fragment surrounding point P_i.

Although positive Δy is assumed in Fig. 5, the similar calculation is possible for negative Δy by tracking the movement of point P_2 instead of P_1. The sign of Δy is estimated by the next inequality.

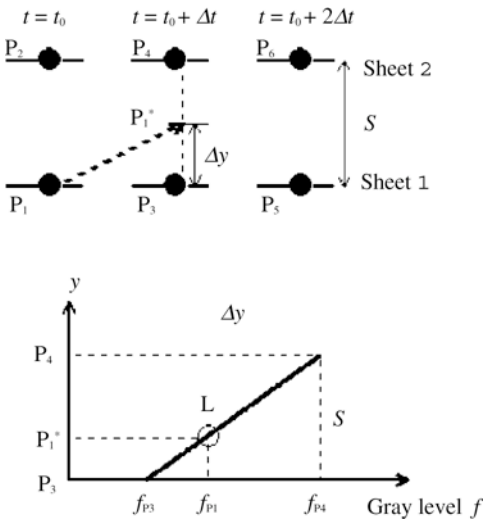

Fig. 5. Calculation of fluid movement toward y-direction.

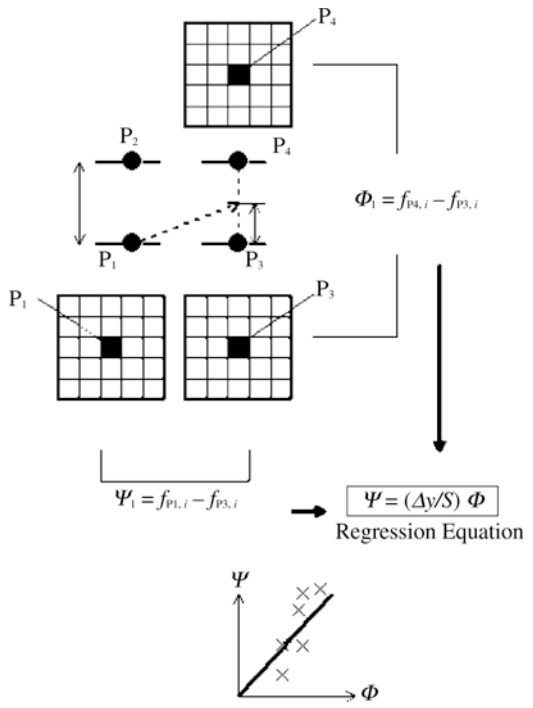

Fig. 6. Regression equation to calculate Δy.

$$\begin{aligned} \Delta y > 0 \quad &\text{if} \quad D_{23} > D_{14} \\ \Delta y < 0 \quad &\text{if} \quad D_{23} < D_{14} \end{aligned} \tag{6}$$

Here

$$\begin{aligned} D_{23} &= \sum | f_{P3} - f_{P2} | \\ D_{14} &= \sum | f_{P4} - f_{P1} | \end{aligned} \tag{7}$$

If the images at successive three times ($t = t_0 \sim t_0 + 2\Delta t$) are used just same as 2-D tracking, a regression equation using three points that are nearer each other is available (Kaga, et al., 1997). In this case, D_{23}, D_{25}, D_{13}, D_{14} and D_{16} are calculated to predict approximate value of Δy from their order of magnitude to select the most adequate regression equation.

4. Simulation Using Visualized Images on One Plane

The performance of the algorithms to calculate velocity components depends directly on the characteristics of visualized images. If the wave length of spatial variation of tracer concentration is much shorter than the light sheet distance S, the assumption of liner concentration change between two light sheets and the algorithms to calculate velocity component normal to the visualized planes will not function well. The performance of the algorithms for images used in an application can be inspected as follows.

Since images obtained on one light sheet (plane I in Fig. 7, for example) can be assumed to approximate images on x-y plane (plane 3) in the point of tracer pattern fineness, the calculations to obtain velocity components can be simulated by using images on one light sheet. When successive three images on plane I are arranged imaginatively as shown in Fig. 7 with arbitrarily given Δy and they are regarded as images on plane 3, the line images ① to ⑥ on imaginary lights can be regarded to correspond to 2-D images on plane I and 2 in a real measurement. Image fragments for calculation are replaced by 1-D image segments Sg.

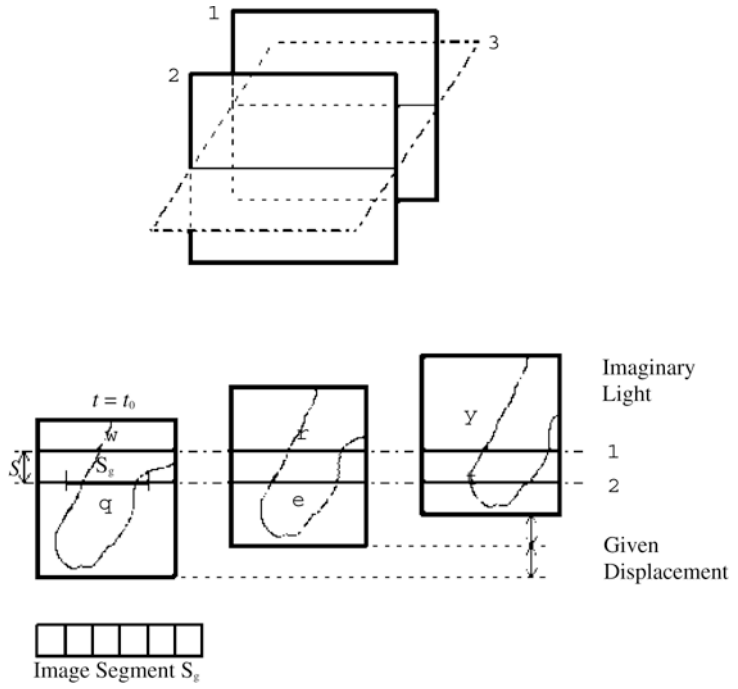

Fig. 7. Imaginary arrangement of images for simulation.

4.1 Calculation of 2-D Components on Visualized Planes

Figure 8 represents a result of the simulation by using visualized images of uniform airflow in a wind tunnel used in the example of application described later. Here the imaginary light sheet distance S is 10 mm (=10 pix), the sampling time step Δt is 1/30 s and x-displacement, Δx, is approximately 10 mm (=10 pix). The length of the image segment that is corresponding to image fragment shown in Fig. 3 in a real measurement is selected to be 450 pix. Δx for 300 samples are calculated by Successive Abandonment using the similarity index of gray level difference corresponding to Eq. (1). Although the average of calculated Δx coincides to the real value in any algorithm, the variance of Δx differes significantly depending on algorithms, as shown in Fig. 8. The performance of usual tracking (1-plane, 2-times) drops significantly when $|\Delta y|$ exceeds $S/2$=5 mm. The performance of the tracking using the images on 2-planes at 2-times (image pairs ① – ③, ① – ④ and ② – ③ in Fig. 4) also drops at the neighborhood of $|\Delta y|$ = 5 mm. The algorithm proposed here (2-planes, 3-times) improves the performance.

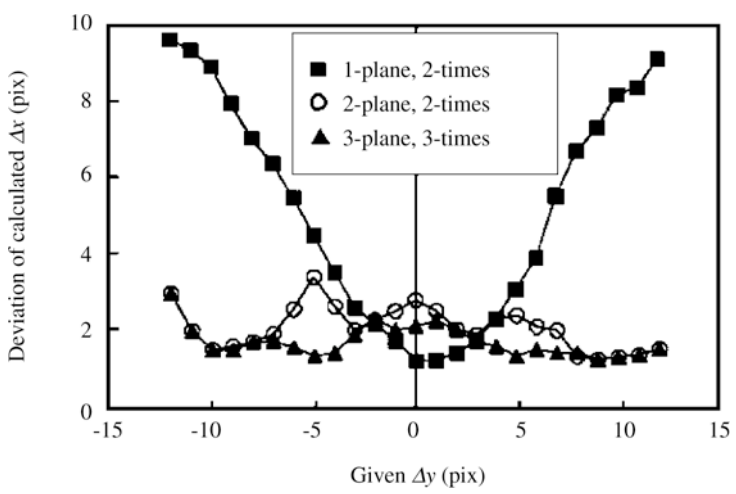

Fig. 8. Standard deviation of calculated Δx (simulation).

4.2 Calculation of Component Normal to Visualized Planes

Figure 9 represents the result of Δy calculation under the same condition as is used in the simulation for 2-D components. Also in this calculation, image segments are used instead of image fragments shown in Fig. 6, just

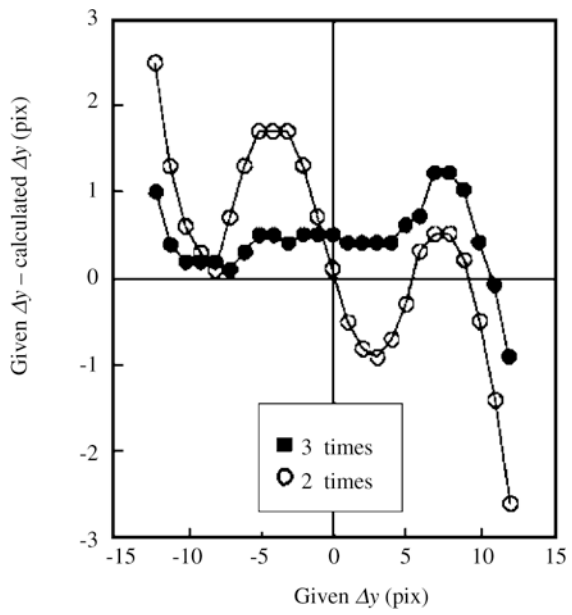

Fig. 9. Calculated Δy (simulation).

same as the calculation of Δx. As shown in Fig. 9, the improved algorithm using images at three times (Kaga, et al., 1997) calculates Δy with the error lower than 1 pix in average value, but the algorithm using images only at two times brings the error of ± 2 pix in Δy calculation.

5. Example of Application

5.1 Experimental Apparatus

The algorithm proposed here is applied to the airflow toward a rectangle prism placed horizontally in a wind tunnel as shown in Fig. 10. The flow was visualized with glycerin mist particles and Ar-laser light sheets of 488 nm and 515 nm in wave length. The optical system used here is illustrated in Fig. 11 and a visualized image is shown in Fig. 12. The thickness of laser light sheet was 1 mm and the distance between two sheets was 10 mm. Images on two planes were recorded on VTRs separately by using two CCD cameras with optical filters. The average velocity was 0.3m/s.

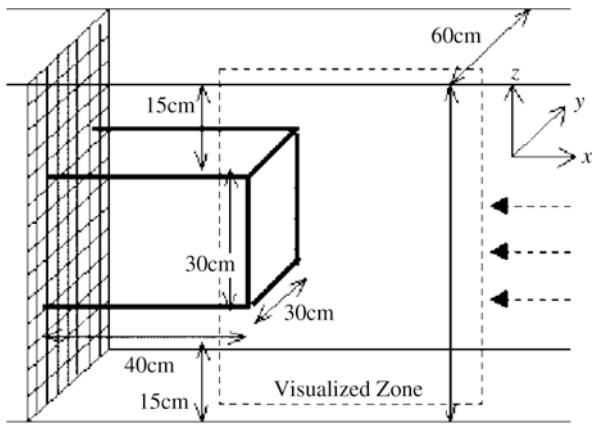

Fig. 10. Wind tunnel for 3-D measurement.

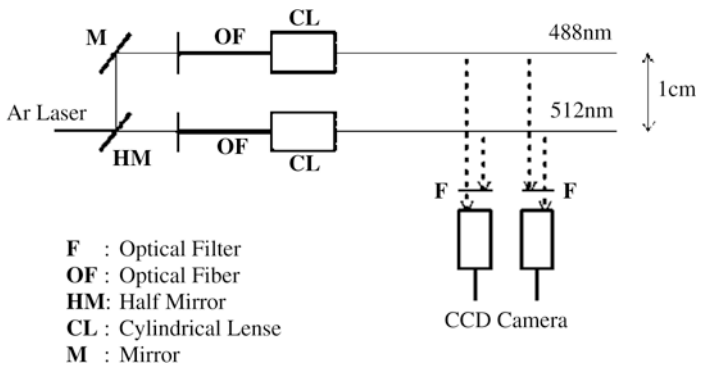

Fig. 11. Optical system for 3-D measurement.

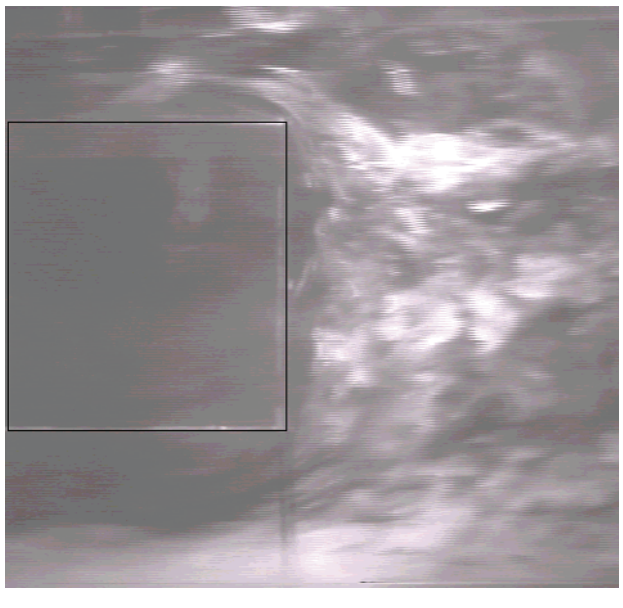

Fig. 12. Visualized image of airflow.

5.2 Adjustments Between Two Camera Images

Because two cameras and two light sheets were used in the experiment, there appeared two factors that were not included in the simulation but had to be adjusted.

One is the adjustment of coordinate difference between two camera images. Here they are correlated by the next quadratic equations and the coefficients, a_1–a_{12}, are calculated with the least square method by using landmark images on both cameras. The error included in the adjustment is about 1 pix.

$$\begin{aligned} \xi_L &= a_1\xi_R^2 + a_2\xi_R\eta_R + a_3\eta_R^2 + a_4\xi_R + a_5\eta_R + a_6 \\ \eta_L &= a_7\xi_R^2 + a_8\xi_R\eta_R + a_9\eta_R^2 + a_{10}\xi_R + a_{11}\eta_R + a_{12} \end{aligned} \tag{8}$$

Here

(ξ_L, η_L) = coordinates on left camera image

(ξ_R, η_R) = coordinates on right camera image

The other was the adjustment of luminous intensity difference between two planes. In our study, the wind tunnel was filled with tracer particles of 32 different levels of uniform concentration before starting a serious of measurement, and the gray levels on two camera images for the same tracer concentration are correlated with a quadratic equation. Equations are prepared for each small segment on images.

5.3 Measurement Result

As shown in Fig. 9, the accuracy of measurement is improved if the images at three times are available to calculate velocity component normal to the visualized planes. But in this experiment, only the sign of Δy could be judged by Eq. (6) from the summation of gray level difference, and the improved algorithm was not applicable. The reason is the tendency that the gray level difference between image fragments on different planes has higher values than the difference between image fragments on the same plane, due to the errors included in the adjustment of luminous intensity difference between two planes.

A part of the measurement result is shown in Fig. 13. Since the accuracy of our method has not yet improved to be high enough to measure instantaneous 3-D velocity distribution due to the immaturity, the obtained result is the time average velocity field calculated from 100 images by eliminating inadequate vectors (Kimura, et al., 1993). The figure shows that 3-D velocity field can be measured by using the algorithm proposed here, but the component normal to the visualized planes seems to include noticeable error compared with the component on visualized planes, and some improvement is required.

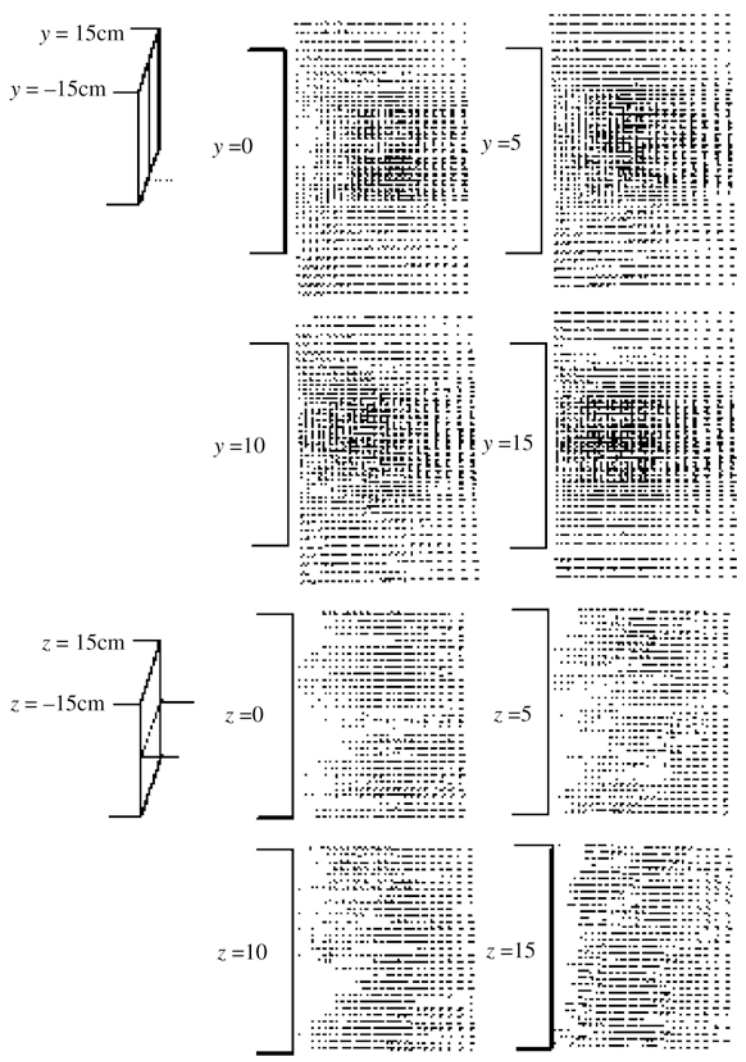

Fig. 13. 3-D velocity distribution of airflow toward a rectangle prism.

6. Concluision

A new 3-D PIV-technique that is applicable to low velocity airflow in a wide space is proposed, and the performance of the technique is inspected with an application and a simulation using real images. It is demonstrated experimentally that 3-D measurement is possible with practical arrangement of cameras and illumination by using the algorithm proposed here. It is also suggested that the luminous intensity difference between two visualized planes is the main source of experimental errors, and some improvement is required.

References

Kaga, A., Inoue,Y. and Yamaguchi, K., Pattern Tracking Algorithm Using Successive Abandonment, J. Flow Visualization and Image Processing, 1-4(1993), 283-296

Kaga, A., Yamaguchi, K., Inoue, Y., Kondo, A., Kamoi, S. and Yamaguchi, T., 3-D Airflow Measurement Coupling Pattern Tracking a nd Spatial Derivative, Proceedings of the First Pacific Symposium on Flow Visualization and Image Processing 1997(Honolulu), (1997.2), 621-626

Kimura, I. and Kohono, Y., Measurement of Three-dimensional Velocity Vectors in a Flow Field Based on Spatio-Temporal Image Cor relation, Proceedings of the Third Triennial International Symposium on Fluid Control, Measurement and Visualization, 1991(San Francisco) , (1991.8), 609-615

Kimura, I., Kuroe, Y. and Ozawa, M., Application of Neural Networks to Quantitative Flow Visualization, J. Flow Visualization a nd Image Processing, 1-4(1993), 261-269

Authors' Profiles

Akikazu Kaga: He received his B.E. degree in 1969, his M.E. degree in 1971 in mechanical engineering, and his D.E. degree in 1985 in Environmental Engineering from Osaka University. He has been working in Osaka University from 1971 as a research associate, and as an associate professor from 1988. His current research interests are airflow measurement using flow visualization and image processing, and numerical simulation of environmental dynamics, especially future prediction of soil acidification due to acid precipitation.

Katsuhito Yamaguchi: He received his B.E. degree in mechanical engineering in 1964 from Osaka University, and his D.E. in Numerical Simulation of Air Distribution in Air-Conditioned Room Space in 1979 from the same university. He worked in the Central Laboratory of Toshiba Company till 1986, which was in the area of nuclear power generation. After that, he worked as an assistant professor in the Department of Environmental Engineering in Osaka University. His research interests in atmospheric environmental engineering include numerical modeling of regional and urban air pollution meteorology.

Yoshio Inoue: He received his B.E. degree in 1973 in mechanical engineering from Osaka Institute of Technology. He has been working in Osaka University from 1971 as a technician, and as a research associate from 1988. His current research interests are airflow measurement using flow visualization and image processing, and automatic recognition of aerosol particles such as asbestos fibers and allergic pollens from microscopic images of specimene using image processing.

Akira Kondo: He received his B.E. degree in 1982 and his M.E. degree in 1984 in environmental engineering from Osaka University. After the M.E. he worked in Matsushita Electric Industrial Co. before taking up his current position as a research associate in Osaka University. His research interest is numerical simulation model of atmospheric boundary layer, the behavior of air pollutants are indoor airflow.